




Effect of Al Elements on the Microstructure and Properties of CoCrNiCuMoAl_x High-Entropy Alloys

KEFENG LU,¹ HONGQI WANG,¹ SHICHONG FAN,¹ YAFAN LIU,¹
NANA GUO,¹ FENGSHI YIN^{1,2}  and JIAN ZHU^{1,3}

1.—School of Mechanical Engineering, Shandong University of Technology, Zibo 255049, China.
2.—e-mail: fsyin@sdut.edu.cn. 3.—e-mail: zhujian@sdut.edu.cn

In CoCrNiCuMo high-entropy alloys (HEAs), the Cu is highly susceptible to segregation, resulting in significant deterioration of plasticity, wear resistance, and corrosion resistance. In this study, Al with atomic ratios of 0, 0.26, 0.56, and 1.00 are added to CoCrNiCuMo to regulate the segregation. The microstructures and composition of CoCrNiCuMoAl_x alloys are characterized by scanning electron microscopy (SEM) and energy dispersive spectrometer (EDS) analysis. The phase composition of the alloys is analyzed by x-ray diffractometry (XRD). The microhardness, compression, friction and wear resistance, and corrosion resistance are also tested to investigate the effect of the Al on the microstructure and properties of the CoCrNiCuMo high-entropy alloys. The results show that, with the addition of Al, the Cu in HEA no longer appears as spheres for large-scale deviations, but form Al-Ni-Cu-rich phases with the Al and Ni in the BCC structure uniformly distributed at the grain boundaries, while the grain size is refined to a certain extent. As the amount of Al addition increases, the values of hardness and compressive strength increase. The CoCrNiCuMoAl_{1.0} alloy possesses the highest hardness and strength of 621.5 HV₅ and 1775 MPa, respectively. Moreover, the wear resistance and corrosion resistance are gradually improved with the increase of Al.

INTRODUCTION

In the harsh marine environment, metal components of marine equipment suffer serious corrosion and wear damage, which leads to the degradation of equipment performance and even some dangerous accidents. Therefore, it is necessary to prepare outstanding wear-resistant and corrosion-resistant coatings on the metal surfaces to solve the problem. High-entropy alloys (HEAs) are a new kind of alloys composed of five or more elements in terms of equal or nearly equal atomic ratios,^{1–3} mainly consisting of simple FCC, BCC, or HCP solid solution. Besides excellent mechanical properties, such as high strength and hardness, some HEA systems containing easily passivated elements also show much better corrosion resistance than traditional

corrosion-resistant materials such as stainless steel.^{4–7} HEAs coating are a recent hotspot of interest, showing a bright future in the protection of metal components in the marine equipment.^{8–11}

At present, there are many kinds of HEAs, generally involving 5–13 kinds of elements, such as Co, Cr, Ni, Mo, Cu, and so on. The roles of each element in HEAs are significantly different. For instance, Co is usually enriched in the inter-dendrite, and the plasticity of HEAs can be improved by "the adhesion bonding effect" of Co. Cr is beneficial for the formation of BCC solid solutions and the enhancement of hardness and strength. Ni can inhibit the defects caused by Al in the process of the preparation of the alloy, and can improve the wear resistance. Because of the larger atomic radius of Mo, the lattice distortion effect and solution strengthening effect are obvious. Cu is good for generating FCC solid solutions, and is uniformly distributed in the grain boundary region helping to improve the ductility of the alloy, Cu also has a

(Received November 30, 2021; accepted March 14, 2022;
published online April 12, 2022)

RESULTS AND DISCUSSION

The XRD diffraction patterns of the CoCrNiCuMoAl x alloy are shown in Fig. 1. The CoCrNiCuMo alloy was composed of FCC, BCC, and Laves solid solution phases, and there were no complex multiphases in the alloys. With increasing Al content, the intensity of the BCC phase diffraction peak gradually increased and the intensity of FCC diffraction peak gradually decreased, which can be attributed to the atomic radius of Al being larger than the atomic radii of the other elements in the alloy. Also, the addition of large-sized atoms increases the atomic radius difference. From the viewpoint of atomic density,²⁰ that of the FCC crystal structure was 74%, while the atomic density of the BCC crystal structure was smaller than that of the FCC structure, only 68%. With increasing Al content, the lattice distortion energy of the alloy also increased, which led to the transformation from the FCC crystal structure to the less dense BCC crystal structure.

Figure 2 shows the SEM backscattered electron images of the CoCrNiCuMoAl x alloy. The arrows point images which are partial enlargements of the left image, where (a), (b), (c), and (d) correspond to the Al contents of $x = 0$, $x = 0.26$, $x = 0.56$, and $x = 1.0$, respectively, and A, B, and C trace the Cu, Mo, and mixed region, respectively. The results of the EDS analysis corresponding to the points are shown in Table II. As can be seen from Fig. 2, the microstructure of the alloy changes significantly with the addition of Al. The phase compositions of the CoCrNiCuMo alloy are: Al-Ni-Cu-rich BCC phase in the form of columnar crystals, spherical Cu-rich FCC phase, and Mo-rich Laves phase. With the increase of the Al content to $x = 0.26$, the alloy begins to have a dendritic tissue morphology, and when $x = 0.56$, the dendritic structure is obvious, and the Cu no longer exists in spherical form, but is based in the dendritic boundary of the BCC phase and the Laves phase of the matrix. When the Al

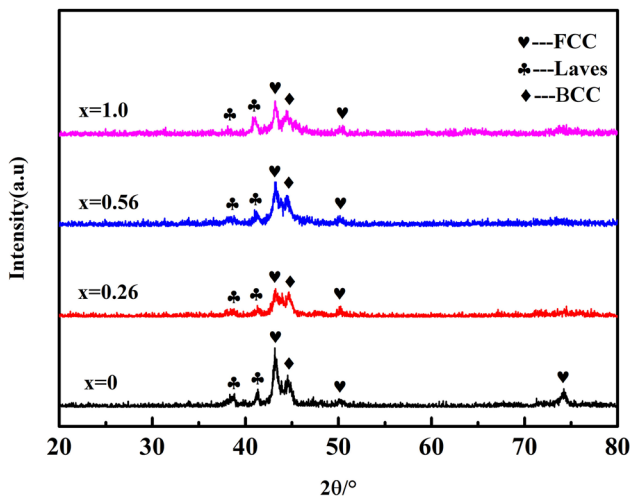


Fig. 1. XRD patterns of CoCrNiCuMoAl x HEAs.

content continues to increase to $x = 1.0$, the grain size becomes more refined and the dendritic matrix undergoes a certain maturation phenomenon. This indicates that, with the increase of Al content, the deviations of Cu are significantly improved until they no longer form a separate phase, and the histomorphology changes from columnar to dendritic crystals.

In the process of non-equilibrium solidification, such as melting, laser cladding, and directional solidification, Cu and the other constituents can be uniformly mixed in the liquid state, but, during the cooling process, solid solution phase formation is related to the atomic radius difference and mixing enthalpy, which can be produced when $-15 \text{ kJ/mol} < \text{mixing enthalpy} < 5 \text{ kJ/mol}$ and the atomic radius difference $\leq 6.6\%$. The enthalpies of mixing between Cu and Co and Cr and Mo are 6 kJ/mol, 12 kJ/mol, and 19 kJ/mol, respectively. Therefore, no intermetallic compounds are formed between them, and the enthalpies of mixing between the remaining elements far exceed the enthalpies of mixing with Cu. It is difficult to form a stable and homogeneous solid solution, which leads to the phenomenon of partial precipitation of Cu in the alloy. The atomic properties of Cu and Ni are closer, thus part of the partial precipitated Cu will have some Ni dissolved in it, which the study of CoCrCuFeNiAl x alloy by Yue et al.²¹ proves. The key technology to eliminate Cu deviations is to achieve complete dissolution of Cu with the solid HEA. The addition of Al improves the solid solution of Cu in the alloy.

The surface scan results of the CoCrNiCuMoAl $_{0.56}$ HEA are shown in Fig. 3. When the Al increases to $x = 0.56$, the Cu gradually fuses with the Al and Ni, indicating that the Al is effectively promoting the dissolution of the Cu and Ni. Therefore, Cu in HEAs no longer appears as spheres for large-scale deviations, but forms Al-Ni-Cu-rich phases with the Al and Ni in the BCC structure uniformly distributed at the grain boundaries. The addition of Al causes the alloy to undergo obvious component subcooling during solidification, resulting in the transformation of the alloy's organization from columnar to dendritic crystals. In addition, the addition of Al also refines the grains of the alloy to a certain extent.

The effect of Al content on the hardness value and compressive strength of CoCrNiCuMoAl x HEAs is shown in Fig. 4, in which the hardness shows a gradual increasing trend with the increase of Al content. CoCrNiCuMo alloys have a minimum hardness value of only 540.5 HV₅. The CoCrNiCuMoAl $_{0.26}$ and CoCrNiCuMoAl $_{0.56}$ alloys have a large increase in hardness values to 572.6 HV₅ and 613.4 HV₅, respectively, but when the Al content increases to $x = 1.0$, the hardness value of the alloy changes less, reaching the highest value to 621.5 HV₅. This is because, with the increase of Al content, the atomic radius difference in the alloy gradually increases, which enhances the lattice

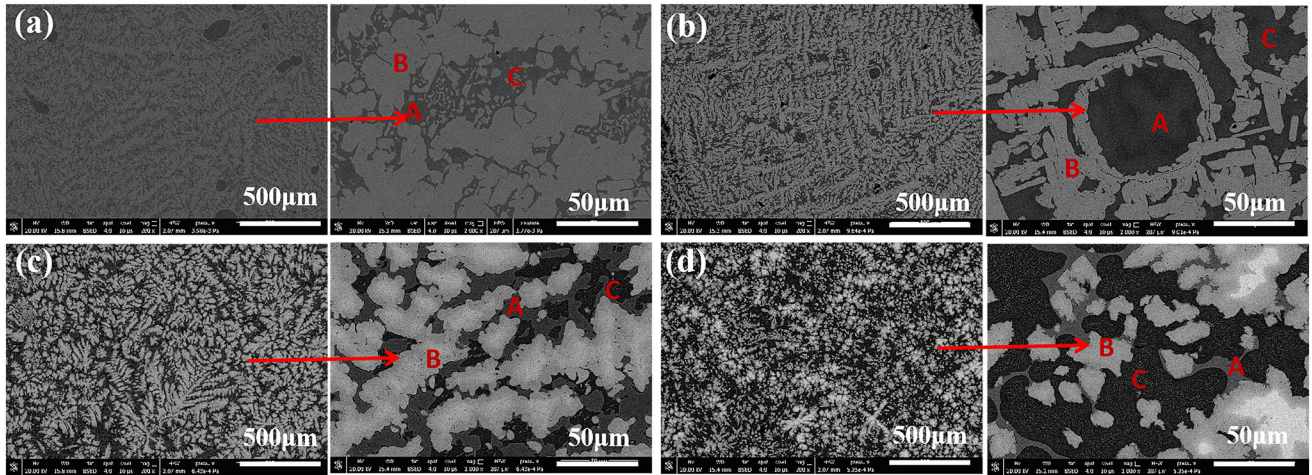


Fig. 2. SEM images of CoCrNiCuMoAl_x HEAs: (a–d) backscattered images for Al 0, Al 0.26, Al 0.56, and Al 1.0, respectively.

Table II. CoCrNiCuMoAl_x HEAs energy spectrum analysis

Number		Cr	Co	Ni	Cu	Mo	Al
x = 0	a—A	2.14	3.47	12.72	81.38	0.29	0
	a—B	19.73	19.24	13.42	1.76	45.86	0
	a—C	17.32	21.22	22.63	15.03	23.80	0
x = 0.26	b—A	3.39	6.08	24.25	62.18	1.29	2.82
	b—B	20.28	20.01	12.22	0	47.14	0.35
	b—C	17.68	25.95	31.42	12.21	10.69	2.06
x = 0.56	c—A	14.47	24.48	32.19	19.40	5.48	3.98
	c—B	19.40	17.04	7.57	0	53.92	0.93
	c—C	5.14	13.57	40.32	29.84	0.67	10.28
x = 1.0	d—A	1.71	4.75	12.39	78.06	0.07	3.02
	d—B	26.39	21.10	7.15	0	42.68	1.68
	d—C	6.98	19.33	35.19	25.12	0.99	12.38

Bold italic entries represents the element most abundant in this region

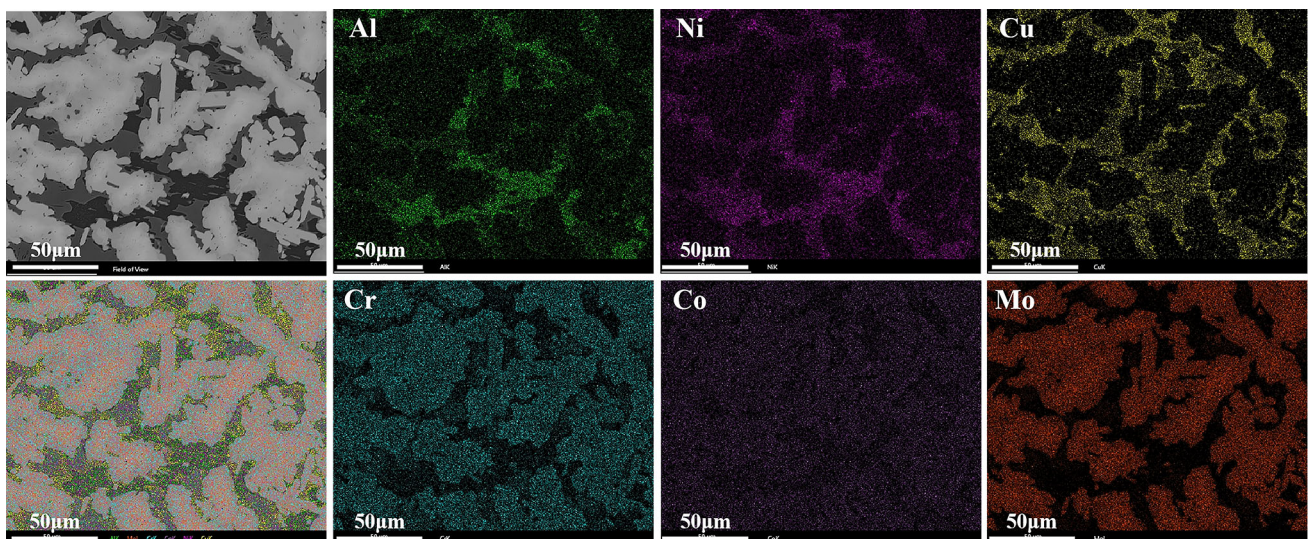


Fig. 3. Surface scan results for CoCrNiCuMoAl_{0.56} HEA.

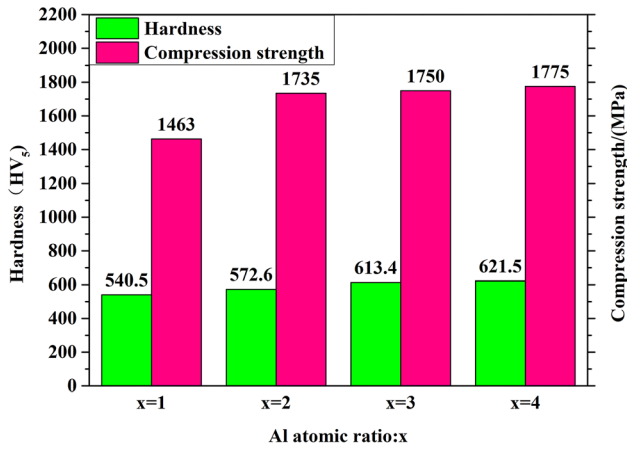


Fig. 4. Micro-hardness and compressive strength curve of CoCrNiCuMoAl_x ($x = 0, 0.26, 0.56, 1.0$) HEAs.

distortion effect in the alloy. At the same time, the addition of Al will make it replace the lattice sites of other atoms, promote the formation of the solid solution phase of the alloy, and enhance the solid solution strengthening effect. As can be seen in Fig. 1, Al can promote the transformation of the FCC structure to the BCC structure, and the BCC structure has a higher hardness than the FCC structure.

In this study, the alloy strength showed a gradual increase with the increase of Al content, and the lowest yield strength of the alloy was 1463 MPa. At this point, the Al element has not yet been added, while the CoCrNiCuMoAl_{1.0} alloy reached the highest value of 1775 MPa. The addition of Al promoted the transformation of the FCC structure to the BCC structure, and the slip surface of the FCC crystal structure was (111), which is easy to slip and has a lower yield strength than the BCC structure, so the yield strength of the alloy gradually increases. In addition, a small amount of Al atoms solid solution into the alloy increases the degree of distortion of the alloy and significantly enhances the solid solution strengthening effect, so the yield strength of the alloy is improved.

Figure 5 shows the compressive fracture morphology of CoCrNiCuMoAl_x HEAs in four groups of $x = 0, 0.26, 0.56, \text{ and } 1.0$. There are many destructive steps and river patterns at the fracture, which in terms of fracture form belong to brittle fracture. As for the CoCrNiCuMoAl_{1.0}, there are many small tough nests at the fracture, indicating that the fracture mechanism of the HEA is tough nest fracture. This is because the increase in Al content enhances the lattice distortion of the internal structure of the alloy, which has a dispersive strengthening effect on it, promoting the formation of tough nests, causing the fracture form of the alloy to change from brittle fracture to ductile fracture.²²

Figure 6 shows the variation curves of the friction coefficient with time for CoCrNiCuMoAl_x HEAs in the reciprocating friction wear experiments. From

the figure, it can be seen that the friction coefficients of each group of alloys shows a trend of increasing and then stabilizing with the increase of experimental time. This is because the wear of the alloy surface is due to fatigue damage, which generates particle fragments to form a third body between the two opposite sides, which will increase the friction coefficient. The friction coefficients of the alloys CoCrNiCuMo and CoCrNiCuMoAl_{1.0} alloys tend to be stable compared to the other groups within 100 s from the beginning of the experiment, indicating that the wear resistance of both two groups is stable. As can be seen from Table III, the friction coefficients of the alloys were about 0.66, 0.68, 0.53, and 0.38 for the CoCrNiCuMo alloy, CoCrNiCuMoAl_{0.26} alloy, CoCrNiCuMoAl_{0.56} alloy, and CoCrNiCuMoAl_{1.0} alloy, respectively. It can be seen that the friction coefficients of the alloys gradually decreased with increasing Al content. This is because, under the long-term friction, the sample surface generates a large amount of heat, and the addition of Al promotes the formation of an oxide layer on the surface of the abrasive marks, which leads to the accumulation of oxide chips and the formation of a high-hardness friction layer, thus reducing the wear between the friction surfaces. In addition, the oxide layer acts as a lubricant, reducing the coefficient of friction and improving the wear resistance of the alloy.

To reveal the effect of Al on the friction and wear properties of the alloy, the wear surface morphology of the wear specimens has been examined by using 3D surface topography and SEM, as shown in Fig. 7. As can be seen, the abrasion marks were deeper when no Al is added, and the depth and width of the abrasion marks decreased with the increase of Al content, while the wear amount decreases, with a large amount of grinding accumulation and protrusion along the edge and the sliding direction of the abrasion marks, and the wear amount is minimized when the content of Al is 1.0. The CoCrNiCuMoAl_x HEAs tissue is fatigued off under the cyclic action of abrasive grains, and plow grooves are formed on the alloy surface tissue, indicating that the wear mechanism is abrasive wear. There are obvious signs of abrasive adherence on the wear surface, and the abrasive chips increase with the increase of Al content. The continuous accumulation of abrasive residues on the surface increased the roughness of the friction surface, which also affects the constant friction coefficient at the later stage of friction fluctuation. In general, the amount of wear and the hardness of the material has a direct relationship, but in the process of frictional wear of the material, the surface and near-surface of the material will be subjected to the pressure of the abrasive vice on it. At the same time, it can impede abrasive vice sliding and cause plastic deformation, and the plowing effect on the abrasive vice will form grooves in the surface of the material. After the reciprocal action of the originally formed grooves, it will be

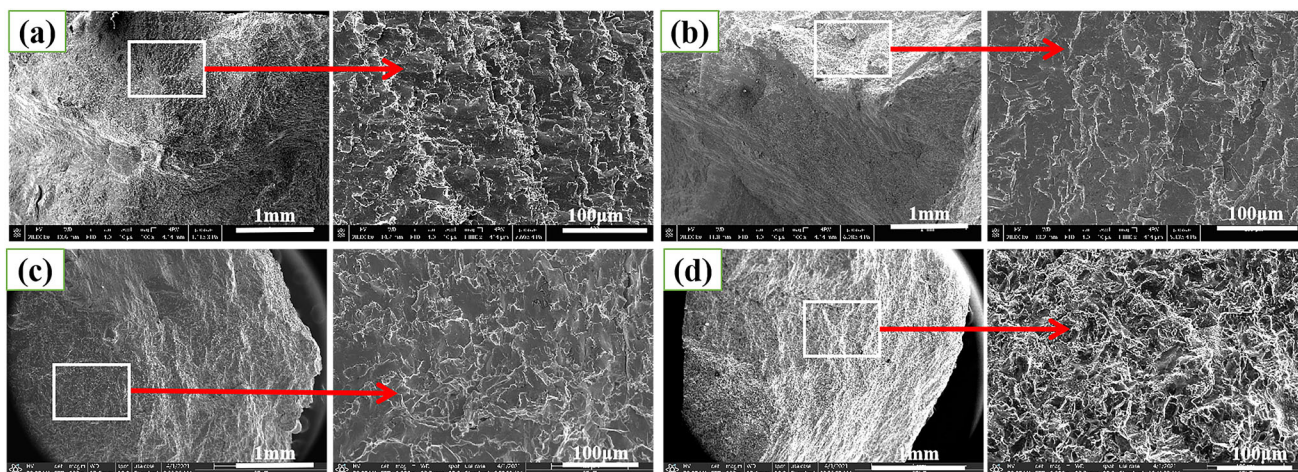


Fig. 5. Compression fracture morphology of CoCrNiCuMoAl_x HEAs (a) $x = 0$, (b) $x = 0.26$, (c) $x = 0.56$, (d) $x = 1.0$.

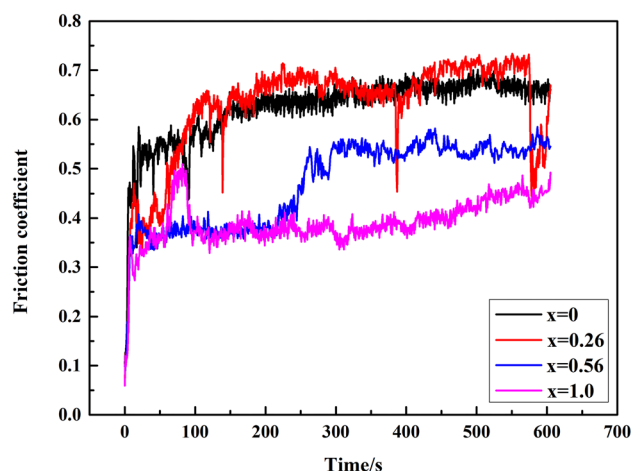


Fig. 6. Friction coefficient versus time of CoCrNiCuMoAl_x ($x = 0, 0.26, 0.56, 1.0$) HEAs.

Table III. CoCrNiCuMoAl_x HEAs average friction coefficient

Al atomic ratio	$x = 0$	$x = 0.26$	$x = 0.56$	$x = 1.00$
Friction coefficient	0.68	0.66	0.53	0.38

ground flat and then followed by new grooves. The amount of wear of the material is also related to its plastic deformation. With the increase of Al content, the formation of the BCC phase will be promoted, the hardness of the alloy is increased, and the friction coefficient of the alloy is gradually reduced. Therefore, the wear on the material is reduced.

Figure 8 shows the potential dynamic polarization (Tafel) curves of the CoCrNiCuMoAl_x HEA in 3.5% (mass fraction) NaCl solution at room temperature. It can be seen that the CoCrNiCuMoAl_{1.0} alloy has the best corrosion resistance according to the highest corrosion potential and the lowest corrosion current density. The self-corrosion potential (E_{corr})

and self-corrosion current density (I_{corr}) are two important parameters of the kinetic potential polarization curve, in which the larger self-corrosion potential indicates the better corrosion resistance of the material in that environment, and the corrosion current density has a positive correlation with the corrosion rate of the alloy with the same exposed area.²³ The self-corrosion potential and self-corrosion current density are obtained by using the extrapolation method, and are listed in Table IV. With the increase of Al content, the self-corrosion potential of CoCrNiCuMoAl_x HEAs gradually increases, and reaches the maximum of -0.434 V when $x = 1.0$. The self-corrosion current density gradually decreases with the increase of Al content, and the self-corrosion current density reaches the minimum at $x = 1.0$, which is 2.42×10^{-6} A/cm². This is because the Cu will be massively polarized when there is no Al added. With the Cu phase as the anode and the surrounding matrix potential difference, accelerating the corrosion of the alloy, with the increase of Al content, alleviates the polarization phenomenon of the Cu. With the positive potential shift, the corrosion resistance of the alloy has been improved. In addition, with the increase of Al content, the lattice distortion energy increases, which also provides the impetus for the formation of passivation films, promotes the formation of a denser passivation film on the alloy surface, increases the width of the passivation zone, and reduces the corrosion rate of the alloy.²⁴

CONCLUSION

Based on CoCrNiCuMo HEAs, the effect of Al content on the microstructure and mechanical properties of the alloy have been studied, and the following main conclusions drawn.

- (1) In CoCrNiCuMo HEAs, With the addition of Al, the presence of Cu is no longer in the form of large-scale deviations in the form of Cu

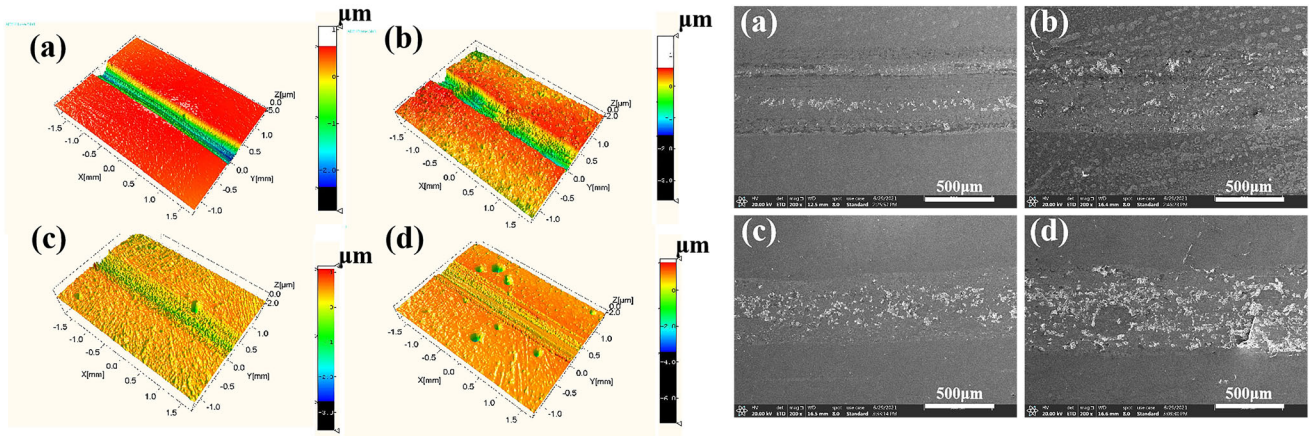


Fig. 7. 3D morphology and SEM images of CoCrNiCuMoAl_x HEAs: (a) $x = 0$, (b) $x = 0.26$, (c) $x = 0.56$, (d) $x = 1.0$.

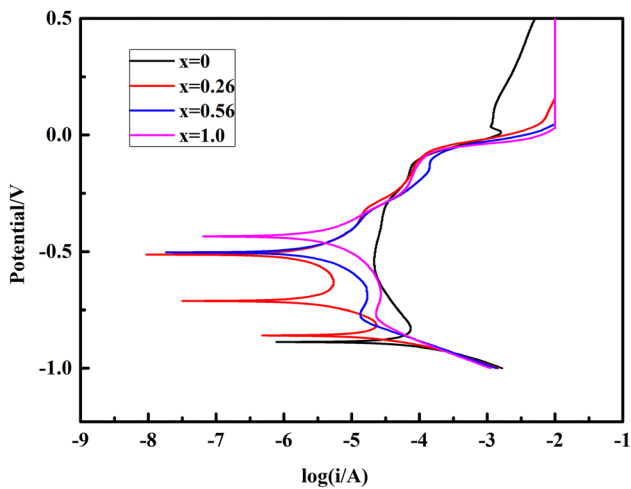


Fig. 8. Potentiodynamic polarization curves of the CoCrNiCuMoAl_x HEAs in a 3.5 wt.% NaCl solution.

Table IV. Corrosion potential (E_{corr}) and corrosion current density (I_{corr}) of CoCrNiCuMoAl_x HEAs

Al atomic ratio	$E_{\text{corr}}/\text{mV}$	$I_{\text{corr}}/(\text{A}/\text{cm}^2)$
$x = 0$	-0.890	5.38×10^{-5}
$x = 0.26$	-0.860	1.67×10^{-5}
$x = 0.56$	-0.506	3.44×10^{-6}
$x = 1.00$	-0.434	2.42×10^{-6}

spheres, but it forms Al-Ni-Cu-rich phases with Al and Ni in the BCC structure uniformly distributed at the grain boundaries. And the microstructure of the alloy changes from columnar crystals to dendritic crystals, while the addition of Al also makes the grains of the alloy refine to a certain extent.

- (2) With the increase of Al content, the hardness and yield strength of the CoCrNiCuMoAl_x HEAs show a gradual increase. The maximum hardness and strength are 621.5 HV₅ and

1775 MPa, respectively, at the Al content of $x = 1.0$.

- (3) With the increase of Al content, the friction coefficient of the CoCrNiCuMoAl_x HEAs gradually decreases, and the wear resistance and corrosion resistance of the alloy gradually increase, indicating that the appropriate amount of Al can improve the wear resistance and corrosion resistance of the alloy.

ACKNOWLEDGEMENTS

This work was supported by National Natural Science Foundation of China (No. 52004154) and Natural Science Foundation of Shandong Province, China (No. ZR2020QE002)

CONFLICT OF INTEREST

The authors declare that they have no conflicts of interest.

REFERENCES

- B. Cantor, I.T.H. Chang, P. Knight, and A.J.B. Vincent, *Mater. Sci. Eng. A* 375(1), 213. (2004).
- G.R. Li, M. Liu, H.M. Wang, D. Zhang, F. Tang, C.W. Wang, Y.T. Zhao, G. Chen, and X.Z. Kai, *JOM* 72(6), 2332. (2020).
- T. Park, and J.H. Kim *JMRTAL* 9(4), 7551. (2020).
- Z. Wang, Q. Wu and W. Zhou, *Scr. Mater* 162, 468. (2019).
- H. He, B. Wang, S. Lan, P.C. Ruff Jacob, C. Sun, M. Naeem, C.T. Liu and X.L. Wang, *JOM* 73(11), 3285. (2021).
- J.-W. Yeh, S.-K. Chen, S.-J. Lin, J.-Y. Gan, T.-S. Chin, T.-T. Shun, C.-H. Tsau, and S.-Y. Chang, *Adv. Eng. Mater* 6(5), 299. (2004).
- W. Zhang, P.K. Liaw, and Y. Zhang, *Sci. China Mater.* 61(1), 2. (2018).
- S. Praveen, and H.S. Kim, *Adv. Eng. Mater.* 20(1), 1. (2018).
- J.Y. He, W.H. Liu, H. Wang, Y. Wu, X.J. Liu, T.G. Nieh, and Z.P. Lu, *Acta Mater.* 62(1), 105. (2014).
- Y. Lu, X. Gao, L. Jiang, Z. Chen, T. Wang, J. Jie, H. Kang, Y. Zhang, S. Guo, H. Ruan, Y. Zhao, Z. Cao, and T. Li, *Acta Mater.* 124, 143. (2017).
- H. Jiang, L. Jiang, and D. Qiao, *JMRTAL* 33(7), 712. (2016).
- Y. Yu, N. Xu, S. Zhu, Z. Qiao, J. Zhang, J. Yang, and W. Liu, *JMRTAL* 69(10), 48. (2021).
- K.N. Campo, C.C. de Freitas, L. Fanton, and R. Caram, *JMRTAL* 52(17), 207. (2020).

14. Y. Zhang, T. Zuo, and Z. Tang, *Prog. Mater. Sci.* 61, 1. (2014).
15. Y. Yu, N. Xu, and S. Zhu, *JMRTAL* 69(10), 48. (2021).
16. Y. Cai, Y. Chen, and Z. Luo, *Mater. Des.* 133, 91. (2017).
17. A. Verma, P. Tarate, and A.C. Abhyankar, *Scr. Mater.* 161, 28. (2019).
18. J.-M. Zhu, J.-L. Meng, and J.-L. Liang, *Rare Met.* 35(5), 385. (2016).
19. H. Zheng, R. Chen, G. Qin, X. Li, Y. Su, H. Ding, J. Guo, and H. Fu, *JMRTAL* 38(3), 19. (2020).
20. Y. Zhou, Y. Zhang, and F. Wang, *J. Alloys Compd.* 466(1), 201. (2008).
21. Y. Zhang, Z. Chen, D. Cao, J. Zhang, P. Zhang, Q. Tao, and X. Yang, *JMRTAL* 8(1), 726. (2019).
22. C.P. Lee, C.C. Chang, and Y.Y. Chen, *Corros. Sci.* 50(7), 2053. (2008).
23. B. Li, P. Kun, and A. Hu, *Trans. Nonferrous Met. Soc. China* 23(3), 735. (2013).
24. Y. Shi, B. Yang, P.K. Liaw, M.C. Gao, and J. Qiao, *Metal* 7(2), 43. (2017).

Publisher's Note Springer Nature remains neutral with regard to jurisdictional claims in published maps and institutional affiliations.